Available online at www.sciencedirect.com
SCIENCE DIRECT
Journal of Molecular Catalysis A: Chemical 242 (2005) 18–25
JOURNAL OF MOLECULAR CATALYSIS A: CHEMICAL
www.elsevier.com/locate/molcata

A computational study of alkane hydrogen-exchange reactions on zeolites

Xiaobo Zheng, Paul Blowers *

Department of Chemical and Environmental Engineering, The University of Arizona, P.O. Box 210011, Tucson, AZ 85721-0011, USA

Received 29 May 2005; received in revised form 18 July 2005; accepted 18 July 2005
Available online 24 August 2005

Abstract

In this work, quantum chemical methods were applied to study light alkane hydrogen-exchange reactions on a zeolite cluster, $RH + H_3SiOAlH_2(OH')SiH_3 \rightarrow RH' + H_3Si(OH)AlH_2OSiH_3$. Methane, ethane, propane, and butane reactions were investigated. The reactants, products, and transition state structures were optimized using the B3LYP density functional theory method and the final energies were calculated using CBS-QB3, a complete basis set composite energy method. The computed activation barriers ranged from 28.32 kcal/mol for secondary hydrogen exchange of butane to 33.53 kcal/mol for methane. The relationship between activation energy and deprotonation energy was also investigated and a linear correlation was proposed in this work.

Keywords: Zeolite; Alkane; Hydrogen exchange; CBS method

1. Introduction

Zeolites are crystalline aluminosilicates that have three-dimensional framework structures, which forms uniformly sized nano-pores from 3 to 10 Å. This is the reason that zeolites exhibit selectivity in adsorbing molecules based on molecular size and shape. As a result, zeolites are broadly used as catalysts in the oil refining and petroleum industries in processes, such as hydrocarbon catalytic cracking, isomerization, alkylation of hydrocarbons, and alcohol conversion to gasoline [1–4]. The fundamental components of zeolite catalytic activity are the Brønsted acidic sites. They are formed when a silicon atom, which has a formal valency of four, is replaced by another atom like aluminum with a valency of three. A proton is attached to the oxygen atom connecting the silicon and its aluminum atom neighbor, resulting in a chemically stable Si–(OH)–Al structure. Si–O and Al–O bonds have considerable covalency, resulting in a relatively weak O–H bond, which is the fundamental reason for the high acidity of the attached proton and for the creation of a good catalyst [5].

Because of the complicated reaction mechanisms and various simultaneous reaction paths, hydrocarbon catalytic reactions on zeolites are very difficult to study experimentally [6,7]. On the other hand, the dramatic increase of computer speed has greatly increased the ability to apply computational tools for investigating large systems in the last decade. Particularly, the development of fast and accurate density functional theory (DFT) methods has extrapolated the computational applications to even more complicated systems. Density functional theory has been widely applied by chemists and physicists to study the electronic structure of solids in the past 30 years [8–20]. Computational studies of chemical reaction systems with DFT have become very popular because the methods are quite reliable and only have medium computational demands compared to ab initio molecular orbital theory calculations.

When applying a computational method to investigate heterogeneous zeolite reactions, the first step is to choose a cluster model to represent the local environment around the zeolitic proton [21]. Several cluster models are commonly used to represent zeolite catalysts. The differences are the number of tetrahedral (T) molecules (Al and Si) included and the termination of the linking bonds (−H or −OH). H_3Si–O–AlH_2–(OH)–SiH_3, a T3 cluster model cluster model, has been applied extensively to investigate hydrocarbon heterogeneous reactions [22–27]. The acidic hydrogen and aluminum atom distance and the acidic H–O bond vibration frequency results of this cluster model have excellent agreement with available experimental data [28–32]. Also, this cluster model has been applied

* Corresponding author. Tel.: +1 520 626 5319; fax: +1 520 621 6048.
E-mail address: blowers@engr.arizona.edu (P. Blowers).

1381-1169/$ – see front matter © 2005 Elsevier B.V. All rights reserved.
doi:10.1016/j.molcata.2005.07.029

successfully to study methane and ethane heterogeneous reactions on zeolites [22,23]. Furthermore, this cluster model has a deprotonation energy close to those found for high-silica acidic zeolites, around 295.4 kcal/mol [7,33]. Therefore, the $H_3Si–O–AlH_2–(OH)–SiH_3$ T3 cluster is used to simulate the zeolite surface in this work.

The alkane hydrogen-exchange reaction seems to be trivial to study at first look. However, the reaction is important because the relatively simple reaction pathway and activation barrier can be studied experimentally rather easily, which can then, in turn, be used to evaluate the choice of computational methods. The zeolite catalytic hydrogen exchange of methane and ethane has been investigated by several groups using different computational approaches [26,27,34–39]. But the activation energies obtained are always off by at least 3 kcal/mol from the experiments, depending on the different choice of zeolite cluster models and computational methods. Other researchers have studied the propane hydrogen-exchange reaction [38,40], while there have been no reported results for the butane reaction. The hydrogen exchange of propane and butane are included because they are the simplest alkanes where the hydrogen exchange on secondary atoms can be observed. In this work, quantum chemical methods were applied to study hydrogen-exchange reactions of methane, ethane, propane, and butane with a T3 zeolite cluster.

2. Computational methods

The well-known B3LYP method uses Becke's three-parameter density functional [41] and Lee et al.'s functional [42] to describe gradient-corrected correlation effects. It has been validated to give results similar to that of the more expensive MP2 theory for molecular geometry and frequency calculations [43,44]. In this work, the geometry optimizations of the reactants, products and transition state structures were carried out using the B3LYP method combined with a moderate basis set, 6–31 g*.

Some researchers have pointed out that the calculated activation energies strongly depend on the level of the final energy calculations and less on the level of the geometry optimization [14,45,46]. Therefore, it is a good choice to perform the geometry optimizations at a relatively lower level, B3LYP/6–31 g* in this work, and the final energy calculations at a higher level, CBS-QB3, a complete basis set composite energy method [47–53]. Composite energy methods are composed of a series of single point energy calculations whose results are then combined to obtain a highly accurate energy at a reduced computational cost. The CBS-QB3 method was proposed by Montgomery et al. [52]. For the G2 test set [54] of first- and seond-row molecules, the mean absolute error was decreased to 0.87 kcal/mol for the CBS-QB3 method compared with 1.37 kcal/mol for the G2 method [55]. In this work, the B3LYP/6–31 g* method is used to perform geometry and frequency calculations in order to reduce computational costs over the CBS-QB3 formalism.

All the calculations were performed with the Gaussian 98 [56] software package, and all the structures were fully optimized without any geometry constraints at the B3LYP/6–31 g* level. The products and reactants were verified with frequency calculations to be stable structures, and the transition states were tested to ensure they were first-order saddle points with only one negative eigenvalue. Additionally, intrinsic reaction coordinate (IRC) calculations proved that each transition state linked the correct products with reactants. Zero point vibrational energies (ZPVE) were obtained from harmonic vibrational frequencies calculated at the B3LYP/6–31 g* level with a scaling factor of 0.9806 [57].

3. Results and discussions

3.1. Methane hydrogen-exchange reaction

$$CH_3Hz + H_3SiOAlH_2(OH')SiH_3 \rightarrow CH_3H' + H_3Si(OHz)AlH_2OSiH_3$$

The methane hydrogen-exchange reaction was previously studied by this group [22] and is briefly discussed here to set up the analysis in this work. In the reaction schematic above, Hz represents the hydrogen exchanged from the CH_4 reactant and H′ represents the protonic hydrogen from the zeolite cluster. Fig. 1 shows the transition state structure for the methane hydrogen-exchange reaction calculated at the B3LYP/6–31 g* level. The structure clearly has C_s symmetry obtained without any symmetry constraints applied for the optimization step. The protonated carbon atom stays in the main plane of zeolite cluster and becomes a penta-coordinated structure. The two hydrogen atoms—H′, the acidic proton from the zeolite cluster and Hz, the exchange hydrogen from the methane molecule, stay in the middle of the carbon and two zeolite oxygen atoms, which indicates the formation of one C–H bond and breaking of the other. In the reaction process, the right oxygen of the cluster acts as a Brønsted acid, which donates a proton. The left oxygen acts as a Lewis base, which receives the hydrogen atom from methane molecule.

Selected bond lengths and angles for the transition state structure are reported in Table 1 along with a comparison to previous computational results from Esteves et al. [40] and Ryder et al.

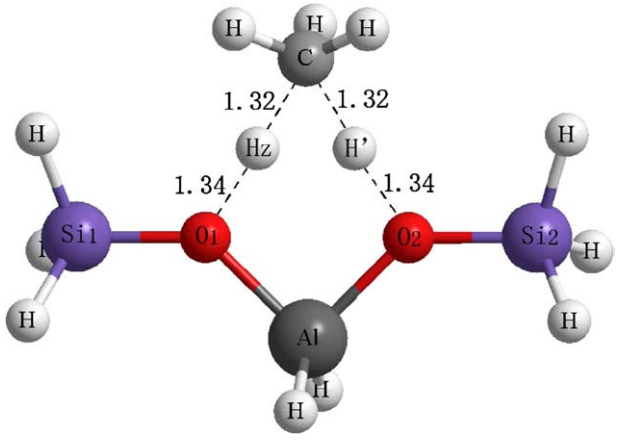

Fig. 1. Calculated transition state structure for the methane hydrogen-exchange reaction on a zeolite cluster (units in Å).

Table 1
Selected bond lengths and angles of the methane hydrogen-exchange reaction transition state structure

	This work	Esteves et al.	Ryder et al.
Geometry optimization	B3LYP/6–31 g*	B3LYP/6–31 g*	BH&HLYP/6–31 g**++
Energy calculation	CBS-QB3	B3LYP/6–31 g**	BH&HLYP/6–31 g**++
Cluster size	T3	T3	T5
R(H′O_2) (Å)	1.34	1.31	1.41
R(HzO_1) (Å)	1.34	1.31	1.41
R(C′H′) (Å)	1.32	1.34	1.28
R(C′Hz) (Å)	1.32	1.34	1.28
R(AlO_1) (Å)	1.86	1.82	1.75
R(AlO_2) (Å)	1.86	1.73	1.75
A(O_1AlO_2) (°)	90.27	91.40	95.70
ν_{TST} (cm^{-1})	1700i	–	1435i
E_a (kcal/mol)	33.53	32.30	40.00

[38]. The negative frequency corresponding to the hydrogen-exchange mode is 1700 cm^{-1}. The activation energy obtained using the CBS-QB3 composite energy method is 33.53 kcal/mol. Other researchers have studied this reaction using computational methods and the calculated activation energies range from 30 to 40 kcal/mol depending on the computational methods and the size of zeolite cluster [37,38,40,58–60]. The experimental study from Larson et al. reported the activation energy for methane H/D exchange to be 33.40 kcal/mol [61]. Our calculated activation energy has an absolute error of only 0.13 kcal/mol compared with the experimental data. This agreement proves our choice of zeolite cluster and computational method is valid. In 1999, Schoofs et al. reported an experimental activation energy of 29.19–35.89 kcal/mol (122–150 kJ/mol) for methane H/D exchange reaction [62]. Our calculation result agrees with this experimental data as well.

3.2. Ethane hydrogen-exchange reaction

$$CH_3CH_2Hz + H_3SiOAlH_2(OH')SiH_3 \rightarrow CH_3CH_2H' + H_3Si(OHz)AlH_2OSiH_3$$

Fig. 2 depicts the calculated transition state structure for the hydrogen-exchange reaction of ethane using the B3LYP method. Similar to the transition state of the methane reaction, the structure keeps its symmetry along the C′–C–Al plane. The protonated carbon atom C′ stays in the main plane of the zeolite cluster and becomes a penta-coordinated structure while the other carbon atom keeps its tetrahedral structure. The proton from the zeolite cluster, H′, and the exchange hydrogen from the ethane molecule, Hz, stay between the C′ carbon atom and the two zeolite oxygen atoms, indicating the formation of a C′–H′ bond and breaking of the C′–Hz bond.

Selected bond lengths and angles for the transition state structure are reported in Table 2 along with a comparison with previous computational results from Esteves et al. [40] and Ryder et al. [38]. The negative frequency corresponding to the hydrogen-exchange mode is 1561 cm^{-1}. The activation energies obtained

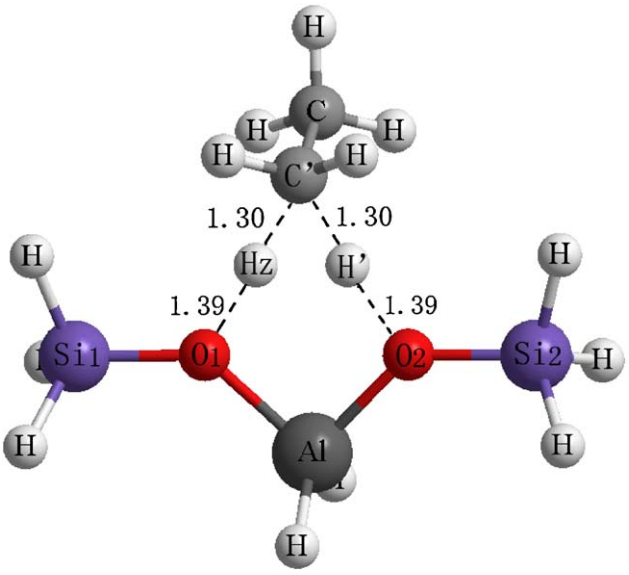

Fig. 2. Calculated transition state structure for the ethane hydrogen-exchange reaction on a zeolite cluster (units in Å).

using the CBS energy is 31.01 kcal/mol. The barrier is relatively lower than that of methane, indicating ethane hydrogen exchange is more favorable than methane. Unfortunately, there is no experimental activation energy available for direct comparison.

3.3. Propane hydrogen-exchange reaction

$$CH_3CH_2\underline{\mathbf{C}}H_2Hz + H_3SiOAlH_2(OH')SiH_3 \rightarrow CH_3CH_2\underline{\mathbf{C}}H_2H' + H_3Si(OHz)AlH_2OSiH_3$$

$$CH_3\underline{\mathbf{C}}HHzCH_3 + H_3SiOAlH_2(OH')SiH_3 \rightarrow CH_3\underline{\mathbf{C}}HH'CH_3 + H_3Si(OHz)AlH_2OSiH_3$$

Table 2
Selected bond lengths and angles of the ethane hydrogen-exchange reaction transition state structure

	This work	Esteves et al.	Ryder et al.
Geometry optimization	B3LYP/6–31 g*	B3LYP/6–31 g*	BH&HLYP/6–31 g**++
Energy calculation	CBS-QB3	B3LYP/6–31 g**	BH&HLYP/6–31 g**++
Cluster size	T3	T3	T5
R(H′O_2) (Å)	1.39	1.36	1.47
R(HzO_1) (Å)	1.39	1.36	1.49
R(C′H′) (Å)	1.30	1.32	1.26
R(C′Hz) (Å)	1.30	1.32	1.28
R(AlO_1) (Å)	1.85	1.83	1.75
R(AlO_2) (Å)	1.85	1.83	1.75
A(O_1AlO_2) (°)	90.56	91.60	95.60
ν_{TST} (cm^{-1})	1561i	–	1147i
E_a (kcal/mol)	31.01	32.30	40.70

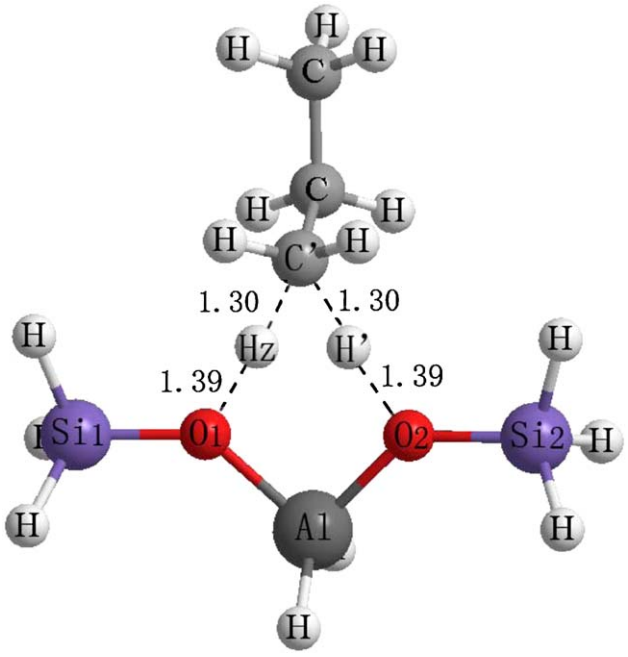

Fig. 3. Calculated transition state structure for the propane primary carbon hydrogen-exchange reaction on a zeolite cluster (units in Å).

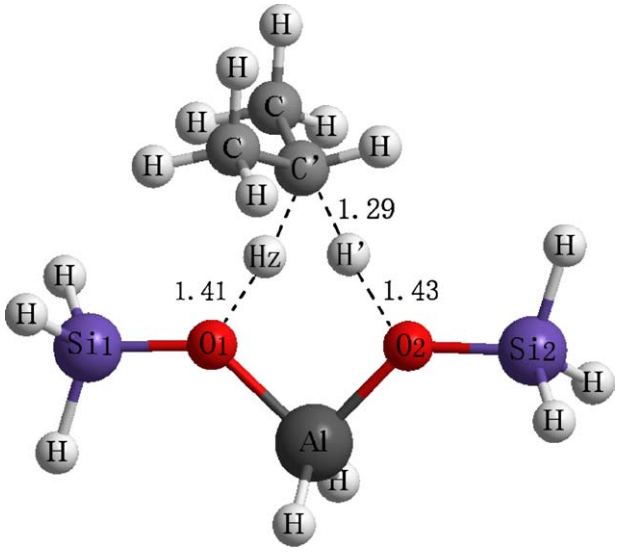

Fig. 4. Calculated transition state structure for the propane secondary carbon hydrogen-exchange reaction on a zeolite cluster (units in Å).

The propane hydrogen-exchange reaction can take place at either the primary carbon or the secondary carbon shown above. The bold underlined carbon atom indicates the place where hydrogen exchange takes place. The calculated transition state structure of primary carbon hydrogen exchange with the B3LYP method is depicted in Fig. 3. Similar to the transition state structures of methane and ethane reactions, symmetry along C–Al plane is observed. In Table 3, selected bond lengths and angles for the transition state structure are reported along with a comparison to previous computational results from Esteves et al. [40] and Ryder et al. [38]. The negative frequency corresponding to the hydrogen-exchange mode is 1549 cm^{-1}. The activation energy is 30.40 kcal/mol and is relatively lower than the calculated results from Esteves and Ryder, which are 32.20 and 40.50 kcal/mol, respectively. The experimental activation energy reported by Stepanov et al. is 25.84 ± 1.67 kcal/mol [63]. Our calculation is only 3 kcal/mol higher than the maximum experimental data and much closer than those from Esteves and Ryder.

The calculated transition state structure of secondary carbon hydrogen exchange with the B3LYP method is shown in Fig. 4. For the first time, the transition state structure does not keep the symmetry as seen from the methane, ethane, and propane primary carbon hydrogen-exchange reactions. The propane structure tilts to the left side of the zeolite cluster and pushes the Hz atom further away from the C′ atom. As a result, the C′Hz distance is slightly larger than the C′H′ distance, while the distance of HzO1 is slightly less than the distance of $H'O_2$. In Table 4, selected bond lengths and angles for the transition state struc-

Table 3
Selected bond lengths and angles of the propane primary carbon hydrogen-exchange reaction transition state structure

	This work	Esteves et al.	Ryder et al.
Geometry optimization	B3LYP/6–31 g*	B3LYP/6–31 g*	BH&HLYP/6–31 g**++
Energy calculation	CBS-QB3	B3LYP/6–31 g**	BH&HLYP/6–31 g**++
Cluster size	T3	T3	T5
R(H′O_2) (Å)	1.39	1.36	1.50
R(HzO_1) (Å)	1.39	1.36	1.46
R(C′H′) (Å)	1.30	1.32	1.24
R(C′Hz) (Å)	1.30	1.32	1.29
R(AlO_1) (Å)	1.85	1.83	1.75
R(AlO_2) (Å)	1.85	1.83	1.75
A(O_1AlO_2) (°)	90.62	91.70	95.60
ν_{TST} (cm^{-1})	1549i	–	1142i
E_a (kcal/mol)	30.40	32.20	40.50

Table 4
Selected bond lengths and angles of the propane secondary carbon hydrogen-exchange reaction transition state structure

	This work	Esteves et al.	Ryder et al.
Geometry optimization	B3LYP/6–31 g*	B3LYP/6–31 g**	BH&HLYP/6–31 g**++
Energy calculation	CBS-QB3	B3LYP/6–31 g**	BH&HLYP/6–31 g**++
Cluster size	T3	T3	T5
R(H′O_2) (Å)	1.43	1.41	1.55
R(HzO_1) (Å)	1.41	1.38	1.47
R(C′H′) (Å)	1.29	1.30	1.24
R(C′Hz) (Å)	1.30	1.31	1.30
R(AlO_1) (Å)	1.85	1.83	1.76
R(AlO_2) (Å)	1.85	1.83	1.74
A(O1AlO_2) (°)	90.66	91.70	96.10
ν_{TST} (cm^{-1})	1459i	–	1029i
E_a (kcal/mol)	29.83	33.30	39.20

ture are reported with a comparison to previous computational results from Esteves et al. [40] and Ryder et al. [38]. The negative frequency corresponding to the hydrogen-exchange mode is 1459 cm^{-1}. The activation energy is 29.83 kcal/mol, and is again much lower than the calculated results from Esteves and Ryder which are 33.30 and 39.20 kcal/mol. Compared with the experimental activation energy of 27.99 ± 1.67 kcal/mol [63], our calculated result is only 0.17 kcal/mol higher. Our calculated results show that the activation energy of secondary carbon hydrogen-exchange reaction is close to but relatively lower than that of primary carbon. Even though our calculated trend seems opposite to the experimental results of Stepanov et al. [63], the experimental trend could be reversed considering the activation energy difference of primary- and secondary-exchange reactions is only 2.15 kcal/mol, and the relatively large error range ± 1.67 kcal/mol for each reaction. Accounting for the errors, the experimental trend could be reversed and become the same as our calculation results. Also, this trend is the same as that obtained by Ryder et al. [38].

3.4. Butane hydrogen-exchange reaction

$$CH_3CH_2CH_2\underline{C}H_2Hz + H_3SiOAlH_2(OH')SiH_3 \rightarrow CH_3CH_2CH_2\underline{C}H_2H' + H_3Si(OHz)AlH_2OSiH_3$$

$$CH_3CH_2\underline{C}HHzCH_3 + H_3SiOAlH_2(OH')SiH_3 \rightarrow CH_3CH_2\underline{C}HH'CH_3 + H_3Si(OHz)AlH_2OSiH_3$$

Similar to propane, the butane hydrogen-exchange reaction can take place at the primary carbon or the secondary carbon shown above. The calculated transition state structure of primary carbon hydrogen exchange with the B3LYP method is depicted in Fig. 5. Similar to the transition state structures of methane and ethane reactions, symmetry along C–Al plane is observed. In Table 5, selected bond lengths and angles for the transition state structure are reported. The negative frequency corresponding to the hydrogen-exchange mode is 1549 cm^{-1}.

Table 5
Selected bond lengths and angles of the butane primary- and secondary-carbon–hydrogen-exchange reaction transition state structures

	$CH_3CH_2CH_2\underline{C}H_3$	$CH_3CH_2\underline{C}H_2CH_3$
Geomtery optimization	B3LYP/6–31 g*	B3LYP/6–31 g*
Energy calculation	CBS-QB3	CBS-QB3
Cluster size	T3	T3
R(H′O_2) (Å)	1.39	1.45
R(HzO_1) (Å)	1.39	1.42
R(C′H′) (Å)	1.30	1.29
R(C′Hz) (Å)	1.30	1.30
R(AlO_1) (Å)	1.85	1.85
R(AlO_2) (Å)	1.85	1.85
A(O_1AlO_2) (°)	90.63	90.90
ν_{TST} (cm^{-1})	1549i	1418i
E_a (kcal/mol)	29.97	28.32

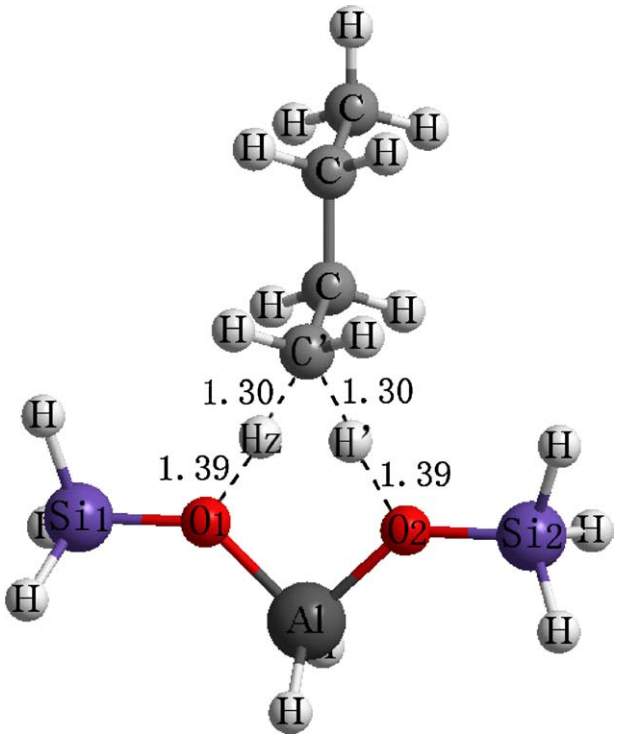

Fig. 5. Calculated transition state structure for the butane primary carbon hydrogen-exchange reaction on a zeolite cluster (units in Å).

The activation energy obtained using the CBS-QB3 method is 29.97 kcal/mol.

The calculated transition state structure of the secondary carbon hydrogen exchange with B3LYP method is shown in Fig. 6. Similar to the propane secondary carbon hydrogen-exchange reaction, the transition state structure does not keep the symmetry as seen for the methane and ethane hydrogen-exchange reactions. As a result, the distances of the acidic proton and secondary carbon, R(C′H′), and exchanging hydrogen and secondary carbon, R(C′Hz),

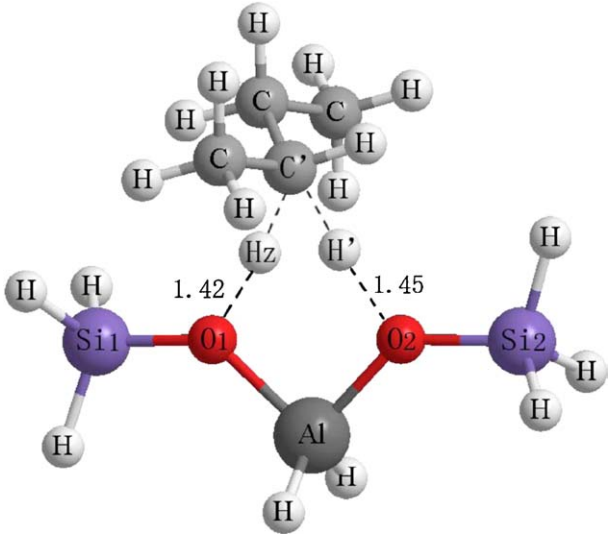

Fig. 6. Calculated transition state structure for the butane secondary carbon hydrogen-exchange reaction on a zeolite cluster (units in Å).

are not identical. In Table 5, selected bond lengths and angles for the transition state structure are reported. The negative frequency corresponding to the hydrogen-exchange mode is 1418 cm^{-1}. The activation energy obtained using the CBS-QB3 method is 28.32 kcal/mol. It is close to, but lower than that of the primary carbon hydrogen-exchange reaction, indicating the butane secondary carbon hydrogen-exchange reaction is relatively easier to take place. This trend is the same as we found for the propane reactions.

For the methane, ethane and propane hydrogen-exchange reactions from Ryder et al., the application of a large T5 cluster containing one Al and four Si atoms to simulate the long-range interactions of a real zeolite catalyst should help increase the accuracy of their calculated results. However, the prohibitive computational cost of introducing five heavy atoms restricts the computational method to a low to medium level, which on the other hand decreases the accuracy. For methane and propane reactions, Ryder's calculated activation energies are 7–11 kcal/mol higher than the experimental values. In this work, we used a relatively smaller T3 cluster, which is still large enough to describe the vicinity of the Brønsted acid site. Also, the system including the T3 cluster and the alkane reactant is still small enough to investigate using high-level computational treatment using the CBS-QB3 composite energy method in this work. As a result, our methane and propane activation energy results are within 3 kcal/mol of the experimental values. The results of Esteves et al. are somewhat unexpected in that the activation energies for primary carbon hydrogen exchange of methane, ethane, and propane are 32.3, 32.3, and 32.2 kcal/mol, almost all identical. The increase of the carbon chain should affect the reaction activation energies, which is not found from their work. Also, the activation energies obtained by Esteves show up to a 7 kcal/mol deviation from experiment because of the relatively lower level B3LYP/6–31 g**++ energy calculation method compared with the CBS-QB3 composite energy method used in this work. This agreement with our results again validates our choice of cluster model and computational method. The BH&HLP/6–31 g**++//BH&HLP/6–31 g**++ (energy calculation method//geometry optimization method) method from Ryder, B3LYP/6–31 g**++//B3LYP/6–31 g**++ method from Esteves and CBS-QB3//B3LYP/6–31 g* from their work also show how the dependence of the calculated activation energies is strongly determined by the level of the final energy calculations and much less on the level of the geometry optimization.

For ethane and butane reactions, even though there is no experimental information available, it is still credible to conclude that our calculated activation energies should be close to the real values considering the results of methane and propane reactions and the similarity of alkane hydrogen-exchange reactions.

3.5. Deprotonation energy and activation energy relationship

The energy required to deprotonate one proton from RH species is the deprotonation energy (E_{dep}).

$$RH \rightarrow R^- + H^+$$

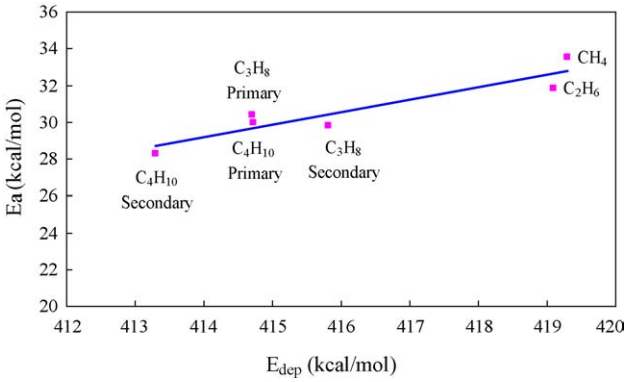

Fig. 7. Hydrogen-exchange reaction activation energy and deprotonation energy relationship for light alkanes.

It is defined as the energy difference between the protonated (RH) and unprotonated (R^-) form [64].

$$E_{dep} = E(R^-) - E(RH)$$

Since the activation barrier for the hydrogen-exchange reaction is directly related to the strength of the R–H bond, we proposed a relationship between the activation energy and the deprotonation energy for light alkanes R–H. Fig. 7 is a plot of the activation energy versus deprotonation energy for methane, ethane, propane, and butane. The deprotonation energies are also obtained at the CBS-QB3//B3LYP/6–31 g* level, the same method used to calculate the activation energies. Since the zeolite acidic OH bond strength stays the same for all of the reactions investigated in this work, the exchange reactions are dominated by the strength of the R–H bonds, which can be described by their deprotonation energies. Therefore, as the deprotonation energy increases, the reaction becomes more difficult to take place and has a higher activation barrier. As long as the reaction mechanism does not alter, the activation energy is linearly correlated to the deprotonation energy. The relationship can be described as:

$$E_a = 0.9935 E_{dep} - 384.32$$

where E_a and E_{dep} are in the units of kcal/mol.

4. Conclusions

In this work, the zeolite-catalyzed hydrogen-exchange reactions of light alkanes including methane, ethane, propane, and butane were studied using quantum chemical methods. The transition state structures of each reaction were optimized at the B3LYP/6–31 g* level, and the energies were obtained using CBS-QB3, a complete basis set composite energy method. The calculated activation energies for methane, ethane, propane primary carbon, and butane primary carbon were 33.53, 31.01, 30.40, and 29.97 kcal/mol. The calculated activation energies for propane and butane secondary carbon hydrogen-exchange reactions were 29.83 and 28.32 kcal/mol, which were relatively lower than that of the primary carbon hydrogen-exchange reactions. Furthermore, a linear relationship was found between

alkane deprotonation energy and its hydrogen-exchange reaction activation barrier.

Acknowledgements

This work was funded by the State of Arizona through the Office of the Vice President for Research at the University of Arizona. Supercomputer time was provided by the National Computational Science Alliance and used the NCSA HP/Convex Exemplar SPP-2000 at the University of Illinois at Urbana-Champaign. Part of the supercomputer time was provided by National Partnership for Advanced Computational Infrastructure and used the IBM pSeries 690 and pSeries 655 at Boston University.

Appendix A. Supplementary data

Supplementary data associated with this article can be found, in the online version, at doi:10.1016/j.molcaa.2005.07.029.

References

[1] B.W. Wojciechowski, A. Corma, Catalytic Cracking: Catalysts, Chemistry, and Kinetics, Dekker, New York, 1986.
[2] I.E. Maxwell, W.H.J. Stork, Introduction to Zeolite Science and Practice, Elsevier, Amsterdam, 1991.
[3] G.A. Olah, A. Molnar, Hydrocarbon Chemistry, John Wiley and Sons Inc., New York, 1995.
[4] I.E. Maxwell, W.H.J. Stork, Studies in surface science and catalysis, in: Introduction to Zeolite Science and Practice, vol. 137, second ed., 2001, p. 747.
[5] E.M. Flanigen, Studies in surface science and catalysis, in: Introduction to Zeolite Science and Practice, vol. 137, second ed., 2001, p. 11.
[6] L.A. Curtiss, M.S. Gordon, Computational Materials Chemistry Methods and Applications, Kluwer Academic Publishers, Dordrecht; Boston; London, 2004.
[7] R.A. van Santen, B. van de Graaf, B. Smit, Studies in surface science and catalysis, in: Introduction to Zeolite Science and Practice, vol. 137, second ed., 2001, p. 419.
[8] A. Bottoni, J. Chem. Soc. Perkin Trans. 2 (1996) 2041.
[9] B.S. Jursic, J. Chem. Soc. Perkin Trans. 2 (1997) 637.
[10] T.N. Truong, T.T.T. Truong, Chem. Phys. Lett. 314 (1999) 529.
[11] T.N. Truong, J. Chem. Phys. 113 (2000) 4957.
[12] J. Lins, M.A.C. Nascimento, Theochem. J. Mol. Struct. 371 (1996) 237.
[13] P.J. Hay, A. Redondo, Y.J. Guo, Catal. Today 50 (1999) 517.
[14] M.V. Frash, V.B. Kazansky, A.M. Rigby, R.A. van Santen, J. Phys. Chem. B 102 (1998) 2232.
[15] J.B. Nicholas, Topics Catal. 4 (1997) 157.
[16] E. Broclawik, H. Himei, M. Yamadaya, M. Kubo, A. Miyamoto, R. Vetrivel, J. Chem. Phys. 103 (1995) 2102.
[17] S.R. Blaszkowski, R.A. Vansanten, J. Phys. Chem. 99 (1995) 11728.
[18] A. Bhan, Y.V. Joshi, W.N. Delgass, K.T. Thomson, J. Phys. Chem. B 107 (2003) 10476.
[19] N.O. Gonzales, A.K. Chakraborty, A.T. Bell, Catal. Lett. 50 (1998) 135.
[20] X. Rozanska, R.A. van Santen, T. Demuth, F. Hutschka, J. Hafner, J. Phys. Chem. B 107 (2003) 1309.
[21] R.A. van Santen, Catal. Today 38 (1997) 377.
[22] X. Zheng, P. Blowers, J. Phys. Chem. A (2005) (in review).
[23] X. Zheng, P. Blowers, J. Mol. Catal. A 229 (2005) 77.
[24] I. Milas, M.A.C. Nascimento, Chem. Phys. Lett. 338 (2001) 67.
[25] E.A. Furtado, I. Milas, J. Lins, M.A.C. Nascimento, Phys. Status Solidi A Appl. Res. 187 (2001) 275.
[26] N.B. Okulik, R.P. Diez, A.H. Jubert, P.M. Esteves, C.J.A. Mota, J. Phys. Chem. A 105 (2001) 7079.
[27] N.B. Okulik, R.P. Diez, A.H. Jubert, J. Phys. Chem. A 108 (2004) 2469.
[28] D. Freude, J. Klinowski, H. Hamdan, Chem. Phys. Lett. 149 (1988) 355.
[29] N.P. Kenaston, A.T. Bell, J.A. Reimer, J. Phys. Chem. 98 (1994) 894.
[30] M.A. Makarova, A.F. Ojo, K. Karim, M. Hunger, J. Dwyer, J. Phys. Chem. 98 (1994) 3619.
[31] L.M. Kustov, V.B. Kazansky, S. Beran, L. Kubelkova, P. Jiru, J. Phys. Chem. 91 (1987) 5247.
[32] M. Trombetta, T. Armaroli, A.G. Alejandre, J.R. Solis, G. Busca, Appl. Catal. A Gen. 192 (2000) 125.
[33] M.V. Frash, R.A. van Santen, Topics Catal. 9 (1999) 191.
[34] S.R. Blaszkowski, M.A.C. Nascimento, R.A. van Santen, J. Phys. Chem. 100 (1996) 3463.
[35] S.A. Zygmunt, L.A. Curtiss, P. Zapol, L.E. Iton, J. Phys. Chem. B 104 (2000) 1944.
[36] V.B. Kazansky, I.N. Senchenya, M. Frash, R.A. van Santen, Catal. Lett. 27 (1994) 345.
[37] V.B. Kazansky, M.V. Frash, R.A. van Santen, Catal. Lett. 28 (1994) 211.
[38] J.A. Ryder, A.K. Chakraborty, A.T. Bell, J. Phys. Chem. B 104 (2000) 6998.
[39] J.M. Vollmer, T.N. Truong, J. Phys. Chem. B 104 (2000) 6308.
[40] P.M. Esteves, M.A.C. Nascimento, C.J.A. Mota, J. Phys. Chem. B 103 (1999) 10417.
[41] A.D. Becke, J. Chem. Phys. 98 (1993) 5648.
[42] C.T. Lee, W.T. Yang, R.G. Parr, Phys. Rev. B 37 (1988) 785.
[43] B.G. Johnson, P.M.W. Gill, J.A. Pople, J. Chem. Phys. 98 (1993) 5612.
[44] C.W. Bauschlicher, H. Partridge, J. Chem. Phys. 103 (1995) 1788.
[45] M.V. Frash, V.B. Kazansky, A.M. Rigby, R.A. van Santen, J. Phys. Chem. B 101 (1997) 5346.
[46] V.B. Kazansky, M.V. Frash, R.A. van Santen, Catal. Lett. 48 (1997) 61.
[47] G.A. Petersson, A. Bennett, T.G. Tensfeldt, M.A. Allaham, W.A. Shirley, J. Mantzaris, J. Chem. Phys. 89 (1988) 2193.
[48] G.A. Petersson, M.A. Allaham, J. Chem. Phys. 94 (1991) 6081.
[49] G.A. Petersson, T.G. Tensfeldt, J.A. Montgomery, J. Chem. Phys. 94 (1991) 6091.
[50] J.A. Montgomery, J.W. Ochterski, G.A. Petersson, J. Chem. Phys. 101 (1994) 5900.
[51] J.W. Ochterski, G.A. Petersson, J.A. Montgomery, J. Chem. Phys. 104 (1996) 2598.
[52] J.A. Montgomery, M.J. Frisch, J.W. Ochterski, G.A. Petersson, J. Chem. Phys. 110 (1999) 2822.
[53] J.A. Montgomery, M.J. Frisch, J.W. Ochterski, G.A. Petersson, J. Chem. Phys. 112 (2000) 6532.
[54] L.A. Curtiss, K. Raghavachari, P.C. Redfern, J.A. Pople, J. Chem. Phys. 106 (1997) 1063.
[55] L.A. Curtiss, K. Raghavachari, G.W. Trucks, J.A. Pople, J. Chem. Phys. 94 (1991) 7221.
[56] M.J. Frisch, G.W. Trucks, H.B. Schlegel, P.M.W. Gill, B.G. Johnson, M.A. Robb, J.R. Cheeseman, T. Keith, G.A. Petersson, J.A. Montegomery, K. Raghavachari, M.A. Al-Laham, V.G. Zakrzewski, J.V. Ortiz, J.B. Foresman, J. Cioslowski, B.B. Stefanov, A. Nanayakkara, M. Challacombe, C.Y. Peng, P.Y. Ayala, W. Chen, M.W. Wong, J.L. Andres, E.S. Replogle, R. Gomperts, R.L. Martin, D.J. Fox, J.S. Binkley, D.J. Defrees, J. Baker, J.P. Stewart, M. Head-Gordon, C. Gonzalez, J.A. Pople, Gaussian Inc., Pittsburgh, PA, 1995.
[57] A.P. Scott, L. Radom, J. Phys. Chem. 100 (1996) 16502.
[58] G.J. Kramer, R.A. Vansanten, C.A. Emeis, A.K. Nowak, Nature 363 (1993) 529.

[59] E.M. Evleth, E. Kassab, L.R. Sierra, J. Phys. Chem. 98 (1994) 1421.
[60] S.R. Blaszkowski, A.P.J. Jansen, M.A.C. Nascimento, R.A. Vansanten, J. Phys. Chem. 98 (1994) 12938.
[61] J.G. Larson, W.K. Hall, J. Phys. Chem. 69 (1965) 3080.
[62] B. Schoofs, J.A. Martens, P.A. Jacobs, R.A. Schoonheydt, J. Catal. 183 (1999) 355.
[63] A.G. Stepanov, H. Ernst, D. Freude, Catal. Lett. 54 (1998) 1.
[64] H.V. Brand, L.A. Curtiss, L.E. Iton, J. Phys. Chem. 97 (1993) 12773.